Journal of Materials Chemistry A

Accepted Manuscript

ROYAL SOCIETY OF CHEMISTRY

www.rsc.org/materialsA

Synthesis and Photovoltaic Properties of Two-dimensional Benzodithiophene-thiophene Copolymers Pendant with Rational Naphtho[1,2-c:5,6-c]bis[1,2,5]thiadiazole Side Chains

Xiaopeng Xu, Kui Feng, Kai Li, Qiang Peng*

Key Laboratory of Green Chemistry and Technology of Ministry of Education, College of Chemistry, and State Key Laboratory of Polymer Materials Engineering, Sichuan University, Chengdu 610065, P. R. China

*To whom correspondence should be addressed: Tel: +86-28-86510868; fax: +86-28-86510868; e-mail: qiangpengjohnny@yahoo.com

Abstract

A series of new two-dimensional copolymers, PBDTT-TABT, PBDTT-TANT and PBDTT-TSNT, with conjugated benzodiathiazole (BT) or naphthobisthiadiazole (NT) side chains were successfully synthesized and characterized towards high performance polymer solar cells (PSCs). The NT unit showed a stronger electron-withdrawing ability and a larger conjugation than those of BT unit, which induced a stronger ICT process between the benzodithiophene (BDT)-thiophene (T) backbone and the conjugated side chain for NT containing copolymers. As a result, PBDTT-TANT and PBDTT-TSNT showed the lower-lying bandgaps and the more red-shifted absorption than those of PBDTT-TABT. The alkylthio modification effect of conjugated side chains was also investigated in this work. This effect just showed a positive role in lowering the HOMO energy level, whereas a negative role in elevating carrier mobility and molecular stacking property in our two-dimensional polymeric system. Bulk heterojunction (BHJ) PSCs were fabricated using these copolymers as the donor materials to evaluate their photovoltaic properties. PBDTT-TABT, PBDTT-TANT and PBDTT-TSBT devices exhibited PCEs of 4.60%, 5.65% and 4.01%, respectively. Despite of V_{oc}, the highest J_{sc}, FF and PCE were achieved for PBDTT-TANT device, which was attributed to its red-shifted absorption, improved carrier mobility and well-defined phase separation. It is interesting that the J_{sc}s, FFs and PCEs of all these devices were elevated significantly when using a solvent vapor annealing (SVA) method. The THF-SVA process would provide a driving force to facilitate to form a much more well-defined surface morphology, resulting in the

enhanced J_{sc} and FF values. PBDTT-TANT device showed the highest PCE of 8.04%, which is the top efficiency for this type of two-dimensional copolymers with donor (D)-donor (D) polymer backbones and donor (D)-acceptor (A) conjugated side chains. Our design strategy would give an instructive meaning in developing high performance two-dimensional polymer donors used in organic photovoltaic applications.

Keywords: Polymer solar cells, Two-dimensional copolymers, Conjugated side chains, Naphthobisthiadiazole, Solvent vapor annealing

1. Introduction

Polymer solar cells (PSCs) have attracted considerable attention in the photovoltaic field because of their potential advantages of low cost, light weight, flexible fabrication and low-temperature solution processing technique.[1] To improve the power conversion efficiency (PCE), significant efforts have been devoted to increasing the open circuit voltage (V_{oc}),[2] short circuit current (J_{sc}),[1a,3] and fill factor (FF).[4] After the bulk heterojunction (BHJ) architecture was introduced into PSCs,[5] the PCE had promptly increased in the past few years from 1% to 10% by designing polymer structures and optimizing device fabrication technologies.[6] Commonly, the active layer of BHJ PSCs contains a phase-separated blend of a donor (D) material and an acceptor (D) material.[1d,5] In most cases, fullerene derivatives were chosen as the acceptor material, such as [6,6]-phenyl-C_{61}-butyric acid methyl ester ($PC_{61}BM$) or [6,6]-phenyl-C_{71}-butyric acid methyl ester ($PC_{71}BM$), which showed relatively weak light-harvest ability in visible light range.[7] Because most of solar flux will be harvested by the donor materials, research efforts on developing new conjugated polymer donors are still the main streams in this field.

Most of the successful polymer donors in PSCs featured a linear and rigid main chain system with flexible side chains.[1c,1d] At the same time, two-dimensional conjugated polymers with conjugated side chains had always been received the extensive concern of the academia.[8] The conjugated side chains would extend the conjugation of the polymer donors, thereby improving the absorption, charge transport, and their device performance.[9] In addition, it could also facilely adjust the

energy levels of the pristine copolymers *via* different conjugated bridges,[10] and enhance the miscibility with fullerene acceptors in BHJ device fabrication.[8b] So far, the two-dimensional polymer donors usually possess some kinds of typical polymeric backbones, such as donor (D)[9a], donor-donor (D-D),[8a,8b,8d,9] donor-acceptor (D-A)[8c,8e] main chain structures. Li *et al.* first designed and synthesized a series of two-dimensional polymer donors using polythiophenes (PT) as the backbone and variable conjugated side chains of bi(phenylenevinylene)[9a], bi(thienylenevinylene)[8a,9b], and phenothiazinevinylene[9c], exhibiting broadened absorption spectra, two-dimensional charge-transport properties, and enhanced device performance. Hou *et al.* first attached two thiophene-conjugated side chains on the skeleton of benzo[1,2-b:4,5-b']dithiophene (BDT), and synthesized a two-dimensional polymer donor with a D-A polymeric backbone.[8c] This strategy has already been employed to constructing high-performance polymer donor materials in PSCs.[6d,11] Tan *et al.* reported a two-dimensional BDT-T copolymer with a D-D polymeric backbone, PTG1, containing 4,7-dithien-5-yl-2,1,3-benzodiathiazole (DTBT) as the conjugated side chains.[8d] PTG1 showed a high hole mobility and a moderate PCE of 4.32%. In order to reduce the bandgap and enhance the absorbance of this type of polymer donors based on BDT-T backbones, isoindigo (ID) unit was introduced instead of benzodiathiazole (BT) unit to develop a new copolymer of PBDT-TID, leading to an enhanced PCE of 6.51% in an inverted device.[12] Recently, Li *et al.* used fluorine substituted BT instead of BT to decrease HOMO energy levels and increase the interchain interaction of PTG1, and synthesized a two-dimensional polymer of

P(BDT-TBTF). P(BDT-TBTF) exhibited an elevated PCE of 6.21% compared to PTG1.[13]

In this work, we designed and synthesized a series of new two-dimensional BDT-T copolymers, PBDTT-TABT, PBDTT-TANT and PBDTT-TSNT, with conjugated BT or naphtho[1,2-c:5,6-c]bis[1,2,5]thiadiazole (NT) side chains (Fig. 1). As is known for acceptor moiety, NT unit is made up of two 1,2,5-thiadiazole rings fused in the skeleton of central naphthalene, which possesses a larger planarity and a stronger electron-withdrawing ability than those of BT unit.[14] The introduction of NT instead of BT would be expected to reduce the bandgap and extend the absorption of the resulting BDT-T copolymers. On the other hand, alkylthio modification have been proved to be an effective approach to further lower the HOMO energy levels and elevate the device performance of BDT-based copolymers in PSCs.[6a,15] Thus, the alkylthio modified thiophene side chains were also introduced on the skeleton of BDT for comparison in this work. As expected, PBDTT-TANT and PBDTT-TSNT with NT side chains showed an enhanced absorption than PBDTT-TABT with BT side chains. However, PBDTT-TABT exhibited a deeper HOMO energy level than those of the other two polymers. Overall, PBDTT-TANT with alkyl modified thiophene side chains showed the best PCE of 8.04% from its conventional PSCs after the solvent vapor annealing (SVA) treatment. The design strategy and results in this work would give an instructive meaning in developing high performance two-dimensional polymer donors in organic photovoltaic applications.

2. Experimental section

2.1 Materials

All reagents were purchased from Aladdin, Alfa Aesar, and Aldrich Co., and used as received without further purification. 2-(2-Hexyldecyl)thiophene (**3a**),[16] 5-(2-hexyldecyl)-2-(tributylstannyl)thiophene (**4a**),[16] 1,4-dibromo-2,1,3-benzothiadiazole (**5a**),[17] 4,9-dibromonaphtho[1,2-c:5,6-c']bis[1,2,5]thiadiazole (**5b**),[14] (2,5-dibromothiophen-3-ylmethyl)phosphonic acid diethyl ester,[8a] 4,8-di(2,3-didecylthiophen-5-yl)-benzo[1,2-b:4,5-b']dithiophene (**10**),[18] were synthesized according to previously reported procedures.

2-[(2-hexyldecyl)thio]thiophene (3b). Under an argon protection, a solution of *n*-butyllithium (20.8 mL, 50 mmol, 2.4 M in hexane) was added dropwise into thiophene (4.2 g, 50 mmol) in 100 mL of dry THF at 0 ^{o}C. After the mixture was stirred at 0 ^{o}C for 1.5 h, sulfur powder (1.6 g, 50 mmol) was added in one portion, and the resulting suspension was then stirred at 0 ^{o}C for another 2 h. Subsequently, 2-hexyldecylbromide (15.2 g, 50 mmol) was added dropwise into above solution. The reaction mixture was stirred overnight at room temperature. After the reaction was finished, ice-water containing NH_4Cl was added to the reactant. The mixture was then extracted with diethyl ether for three times. The combined organic layers were washed with water for another three times, and dried over anhydrous $MgSO_4$. After the removal of solvent, purification was carried out by column chromatography (silica gel; eluent: petroleum ether) to afford compound **3b** (13.90 g, yield: 82%) as colorless oil. ^{1}H NMR (400 MHz, $CDCl_3$, δ/ppm): 7.28-7.26 (m, 1H, ArH), 7.07-7.06 (m, 1H, ArH), 7.96-7.94 (m, 1H, ArH), 2.80-2.78 (d, 2H, J = 15.8 Hz, CH_2), 1.59-1.53 (m, 1H, CH),

1.40-1.25 (m, 24H, CH_2), 0.87-0.84 (m, 6H, CH_3). ^{13}C NMR (100 MHz, $CDCl_3$, δ/ppm): 136.02, 132.63, 128.54, 127.35, 44.24, 39.63, 39.54, 37.63, 32.82, 32.55, 31.96, 31.84, 29.8,7 29.69, 29.51, 29.30, 26.68, 26.56, 22.74, 14.23. Anal Calcd for $C_{20}H_{36}S_2$ (%): C, 70.52; H, 10.65. Found (%): C, 70.33; H, 10.50.

2-[(2-hexyldecyl)thio]-5-tributhylthiophene (4b). Under an argon atmosphere, compound **3b** (1.7 g, 5.0 mmol) was dissolved in anhydrous THF (20 mL) in a three-neck flask. Then, a solution of *n*-BuLi (3 mL, 7.5 mmol, 2.5 M in hexane) was added dropwise with stirring. After the addition was finished, the reaction mixture was stirred for 0.5 hours. $Sn(n\text{-}Bu)_3Cl$ (2.44 g, 7.5 mmol) was subsequently added in one portion to the reactant. The reaction mixture was stirred overnight at room temperature. After that, the reaction mixture was poured into water and extracted twice with dichloromethane. The combined organic layers were dried over anhydrous $MgSO_4$, and the filtrate was concentrated to afford the yellow product. The crude product was purified by column chromatography (silica gel; eluent: petroleum ether) to afford compound **4b** (2.61 g, yield: 83%) as yellowish oil. ^1H NMR (400 MHz, $CDCl_3$, δ/ppm): 7.15-7.14 (m, 1H, ArH), 7.01-7.00 (m, 1H, ArH), 2.82-2.80 (d, 2H, *J* = 15.8 Hz, CH_2), 1.60-1.59 (m, 1H, CH), 1.56-1.54 (m, 4H, CH_2), 1.36-1.07 (m, 38H, CH_2), 0.90-0.87 (m, 15H, CH_3). ^{13}C NMR (100 MHz, $CDCl_3$, δ/ppm): 141.09, 140.91, 135.60, 132.94, 37.69, 32.90, 31.95, 31.88, 29.94, 29.62, 29.59, 29.37, 28.96, 27.27, 26.50, 26.47, 22.73, 22.71, 14.15, 13.67, 10.84. Anal Calcd for $C_{32}H_{62}S_2S_n$ (%): C, 61.04; H, 9.92. Found (%): C, 61.22; H, 9.98.

Compound 6a. Compound **4a** (2.03 g, 3.4 mmol) and compound **5a** (1.0 g, 3.4

mmol) were dissolved in 80 mL toluene, and the mixture was deoxygenated with argon gas for 30 min. The catalytic amount of $Pd(PPh_3)_4$ was then added into the reactant, and the mixture was stirred at 120 °C for 12 h. The mixture was poured into water and extracted with dichloromethane for three times. The combined organic layers were then dried over anhydrous $MgSO_4$. After concentration, the crude product was purified by column chromatography (silica gel; eluent: petroleum ether: dichloromethane = 4:1) to afford compound **6a** (0.35 g, yield: 20%) as a red solid. ^{1}H NMR (400 MHz, $CDCl_3$, δ/ppm): 7.94-7.93 (d, 1H, *J* = 9.1 Hz, ArH), 7.81-7.80 (d, 1H, *J* = 19.4 Hz, ArH), 7.64-7.62 (d, 1H, *J* = 19.3 Hz, ArH), 6.84-6.80 (d, 1H, *J* = 9.1 Hz, ArH), 2.81-2.80 (d, 2H, *J* = 16.7 Hz, th CH_2), 1.75-1.59 (m, 1H, CH), 1.35-1.26 (m, 24H, CH_2), 0.87-0.84 (m, 6H, CH_3). ^{13}C NMR (100 MHz, $CDCl_3$, δ/ppm): 153.81, 151.72, 147.11, 136.04, 132.35, 128.26, 127.47, 126.58, 125.05, 112.40, 40.11, 34.62, 33.24, 33.26, 30.07, 29.78, 29.64, 29.32, 26.67, 22.75, 14.29. Anal. Calcd for $C_{26}H_{37}ON_2Br$ (%): C, 59.87; H, 7.15; N, 5.37. Found (%): C, 60.58; H, 7.36; N, 5.54.

Compound 6b. Compound **6b** was synthesized as a red solid according to the similar route as that for compound **6a** with a yield of 35%. ^{1}H NMR (400 MHz, $CDCl_3$, δ/ppm): 9.02 (s, 1H, ArH), 8.85 (s, 1H, ArH), 8.15-8.14 (d, 1H, *J* = 9.1 Hz, ArH), 6.90-6.89 (d, 1H, *J* = 9.2 Hz, ArH), 2.86-2.84 (d, 2H, *J* = 16.9 Hz, CH_2), 1.75 (br, 1H, CH), 1.35-1.25 (m, 24H, CH_2), 0.89-0.86 (m, 6H, CH_3). ^{13}C NMR (100 MHz, $CDCl_3$, δ/ppm): 153.11, 152.43, 152.14, 151.91, 148.95, 136.27, 129.58, 129.18, 127.67, 126.65, 125.31, 124.12, 120.93, 113.14, 40.15, 34.95, 33.32, 33.25, 32.06, 30.07, 29.68, 29.69, 29.44, 26.66, 22.71, 14.23, 14.15. Anal. Calcd for

$C_{30}H_{37}ON_4S_3Br$ (%): C, 57.22; H, 5.92; N, 8.90. Found (%): C, 57.83; H, 5.45; N, 8.75.

Compound 6c. Compound **6c** was synthesized as a red solid according to the similar route as that for compound **6a** with a yield of 35%. ^{1}H NMR (400 MHz, $CDCl_3$, δ/ppm): 9.06 (s, 1H, ArH), 8.98 (s, 1H, ArH), 8.15-8.14 (d, 1H, *J* = 9.7 Hz, ArH), 7.18-7.17 (d, 1H, *J* = 9.7 Hz, ArH), 2.99-2.97 (d, 2H, *J* = 15.7 Hz, CH_2), 1.72-1.67 (m, 1H, CH), 1.40-1.25 (m, 24H, CH_2), 0.86-0.82 (m, 6H, CH_3). ^{13}C NMR (100 MHz, $CDCl_3$, δ/ppm): 166.74, 165.97, 165.68, 165.33, 154.36, 153.63, 145.67, 143.08, 142.83, 142.78, 140.39, 138.73, 138.04, 134.82, 134.63, 127.46, 57.48, 51.78, 46.89, 45.70, 43.88, 43.43, 43.31, 43.21, 40.33, 39.52, 38.56, 37.63, 36.54, 28.05. Anal. Calcd for $C_{30}H_{37}ON_2BrS_4$ (%): C, 54.45; H, 5.64; N, 8.47. Found (%): C, 54.19; H, 5.79; N, 9.00.

Compound 7a. Compound **4a** (0.1 g, 0.192 mmol) and 2-tributhylthiophene (0.0717 g, 0.192 mmol) were dissolved in 10 mL toluene and the mixture was deoxygenated with argon gas for 30 min. The catalytic amount of $Pd(PPh_3)_4$ was added into the solution, and the mixture was then stirred at 120 °C for 12 h. After that, the mixture was poured into water and extracted with dichloromethane. The combined organic layers were dried over anhydrous $MgSO_4$. After the removal of solvent, the crude product was purified column chromatography (silica gel; eluent: petroleum ether: dichloromethane = 4:1) to afford compound **7a** (0.092 g, yield: 91%) as a red solid. ^{1}H NMR (400 MHz, $CDCl_3$, δ/ppm): 8.08-8.08 (m, 1H, ArH), 7.96-7.95 (d, 1H, *J* = 9.1 Hz, ArH), 7.64-7.62 (d, 1H, *J* = 19.3 Hz, ArH), 7.82-7.80 (d, 1H, *J* = 19.0 Hz,

ArH), 7.76-7.74 (d, 1H, *J* = 19.0 Hz, ArH), 7.43-7.42 (d, 1H, *J* = 12.7 Hz, ArH), 7.20-7.18 (d, 1H, *J* = 12.7 Hz, ArH), 6.85-6.84 (m, 1H, *J* = 9.2 Hz, ArH), 2.82-2.80 (d, 2H, *J* = 16.8 Hz, CH_2), 1.71 (br, 1H, CH), 1.32-1.27 (m, 24H, CH_2), 0.87-0.84 (m, 6H, CH_3). ^{13}C NMR (100 MHz, $CDCl_3$, δ/ppm): 152.61, 152.53, 146.69, 139.53, 137.05, 127.95, 127.67, 127.23, 126.57, 126.49, 126.30, 125.82, 125.24, 124.82, 40.11, 34.73, 33.34, 33.26, 32.02, 30.07, 29.74, 26.77, 22.88, 14.22. Anal. Calcd for $C_{30}H_{40}N_2S_3$ (%): C, 68.65; H, 7.68; N, 5.34. Found (%): C, 68.60; H, 7.73; N, 5.42.

Compound 7b. Compound **7b** was synthesized as a red solid according to the similar route as that for compound **7a** with a yield of 66%. ^{1}H NMR (400 MHz, $CDCl_3$, δ/ppm): 8.90 (s, 1H, ArH), 8.81 (s, 1H, ArH), 8.22-8.21 (m, 1H, ArH), 8.10-8.09 (d, 1H, *J* = 9.2 Hz, ArH), 7.51-7.50 (m, 1H, ArH), 6.89-6.88 (d, 1H, *J* = 9.2 Hz, ArH), 2.85-2.84 (d, 2H, *J* = 16.8 Hz, CH_2), 1.75 (br, 1H, CH), 1.36-1.25 (m, 24H, CH_2), 0.89-0.86 (m, 6H, CH_3). ^{13}C NMR (100 MHz, $CDCl_3$, δ/ppm): 153.13, 152.05, 147.56, 139.07, 136.58, 128.69, 128.28, 128.07, 127.34, 126.55, 122.15, 121.06, 40.27, 34.88, 33.34, 32.02, 30.14, 33.27, 32.05, 30.08, 29.72, 29.64, 29.46, 26.66, 22.77, 14.28, 14.12. Anal. Calcd for $C_{34}H_{40}ON_4S_4$ (%): C, 64.52; H, 6.37; N, 8.85. Found (%): C, 64.13; H, 6.79; N, 8.75.

Compound 7c. Compound **7c** was synthesized as a red solid according to the similar route as that for compound **7a** with a yield of 64%. ^{1}H NMR (400 MHz, $CDCl_3$, δ/ppm): 8.84 (s, 1H, ArH), 8.40 (s, 1H, ArH), 8.04-8.03 (d, 1H, *J* = 7.6 Hz, ArH), 7.88-7.87 (d, 1H, *J* = 9.4 Hz, ArH), 7.43-7.42 (d, 1H, *J* = 12.3 Hz, ArH), 7.15-7.13 (m, 1H, ArH), 7.05-7.04 (d, 1H, *J* = 9.4 Hz, ArH), 2.98-2.96 (d, 2H, *J* =

15.2 Hz, CH_2), 1.75 (br, 1H, CH), 1.47-1.25 (m, 24H, CH_2), 0.89-0.86 (m, 6H, CH_3). ^{13}C NMR (100 MHz, $CDCl_3$, δ/ppm): 152.83, 151.76, 140.37, 139.68, 138.89, 132.08, 128.57, 128.36, 128.05, 127.43, 125.93, 125.54, 124.15, 124.06, 121.72, 121.15, 43.77, 37.88, 36.53, 34.57, 33.59, 32.94, 32.65, 32.05, 31.94, 30.02, 29.76, 29.45, 26.67, 26.58, 24.43, 22.72, 14.24, 14.1. Anal. Calcd for $C_{34}H_{40}ON_4S_5$ (%): C, 61.41; H, 6.06; N, 8.42. Found (%): C, 61.78; H, 6.16; N, 8.79.

Compound 8a. To the mixture of compound **7a** (0.11 g, 0.21 mmol) in 30 mL dry 1,2-dichloroethane. When the solution was cooled to 0 ^{o}C, anhydrous DMF (0.016 g, 0.21 mmol) and $POCl_3$ (0.032 g, 0.33 mmol) were added dropwise slowly in turn under nitrogen atmosphere. The mixture was stirred at 85 °C for 24 h. Then, the mixture was cooled to room temperature, and 30 mL of saturated NH_4Cl solution was added. The mixture was extracted with CH_2Cl_2 for several times, and the combined organic layers were dried over anhydrous $MgSO_4$. After the solvent was removed, the crude product was purified by column chromatography (silica gel; eluent: hexane: dichloromethane = 1:1) to afford compound **8a** (0.063 g, yield: 54%) as a red solid. ^{1}H NMR (400 MHz, $CDCl_3$, δ/ppm): 9.97 (s, 1H, CHO), 8.19-8.18 (d, 1H, *J* = 9.1 Hz, ArH), 8.04-8.03 (d, 1H, *J* = 9.1 Hz, ArH), 7.98-7.96 (d, 1H, *J* = 19.2 Hz, ArH), 7.82-7.81 (m, 2H, ArH), 6.88-6.78 (d, 1H, *J* = 9.2 Hz, ArH), 2.84-2.82 (d, 2H, *J* = 16.7 Hz, CH_2), 1.71 (br, 1H, CH), 1.32-1.27 (m, 24H, CH_2), 0.87-0.84 (m, 6H, CH_3). ^{13}C NMR (100 MHz, $CDCl_3$, δ/ppm): 183.0, 152.84, 152.37, 148.88, 147.99, 143.14, 136.85, 136.56, 128.63, 128.46, 127.67, 127.41, 126.64, 124.36, 123.57, 40.17, 34.87, 33.39, 33.22, 31.94, 29.95, 29.71, 29.64, 29.44, 26.62, 22.75, 14.16. Anal. Calcd for

$C_{31}H_{40}N_2OS_3$ (%): C, 67.35; H, 7.29; N, 5.07. Found (%): C, 67.57; H, 7.25; N, 5.02.

Compound 8b. Compound **8b** was synthesized as a red solid according to the similar route as that for compound **8a** with a yield of 84%. ^{1}H NMR (400 MHz, $CDCl_3$, δ/ppm): 9.99 (s, 1H, ArH), 8.88 (s, 1H, ArH), 8.70 (s, 1H, ArH), 8.20-8.19 (m, 1H, ArH), 8.08-8.07 (d, 1H, *J*=9.1 Hz, ArH), 7.82-7.81 (m, 1H, ArH), 6.87-6.86 (m, 1H, ArH), 2.85-2.84 (d, 2H, *J*=16.8 Hz, CH_2), 1.75 (br, 1H, CH), 1.36-1.30 (m, 24H, CH_2), 0.89-0.86 (t, 6H, CH_3). ^{13}C NMR (100 MHz, $CDCl_3$, δ/ppm): 182.91, 152.91, 152.83, 151.84, 151.55, 148.32, 147.87, 143.85, 136.48, 136.24, 129.27, 128.24, 127.77, 126.74, 125.73, 124.05, 123.82, 123.28, 120.64, 40.28, 34.89, 33.33, 31.91, 30.06, 29.74, 29.66, 29.42, 26.67, 22.78, 14.24, 14.13. Anal. Calcd for $C_{35}H_{42}ON_4S_4$ (%): C, 63.41; H, 6.39; N, 8.45. Found (%): C, 63.79; H, 6.22; N, 8.33.

Compound 8c. Compound **8c** was synthesized as a red solid according to the similar route as that for compound **8a** with a yield of 30%. ^{1}H NMR (400 MHz, $CDCl_3$, δ/ppm): 10.00 (s, 1H, CHO), 9.08 (s, 1H, ArH), 8.89 (s, 1H, ArH), 8.29-8.28 (t, 1H, ArH), 8.17-8.16 (t, 1H, ArH),7.87-7.86 (d, 1H, *J* = 10.0 Hz, ArH), 6.91-6.90 (d, 1H, *J* = 9.0 Hz, ArH), 2.87-2.85 (d, 2H, *J* = 16.8 Hz, CH_2), 1.75-1.74 (m, 1H, CH), 1.36-1.25 (m, 24H, CH_2), 0.86-0.82 (m, 6H, CH_3). ^{13}C NMR (100 MHz, $CDCl_3$, δ/ppm): 182.92, 152.74, 152.66, 151.76, 151.48, 148.29, 147.73, 143.82, 136.46, 136.37, 129.28, 128.51, 127.93, 127.76, 126.57, 125.74, 123.88, 123.56, 123.08, 120.43, 40.12, 34.51, 34.85, 31.96, 31.07, 29.97, 29.16, 29.05, 27.64, 22.04, 14.22, 14.1. Anal. Calcd for $C_{35}H_{40}ON_4BrS_5$ (%): C, 60.66; H, 5.82; N, 8.8. Found (%): C, 61.09; H, 5.69; N, 9.03.

Monomer 9a. (2,5-Dibromothiophen-3-ylmethyl)phosphonic acid diethyl ester (0.078 g, 0.2 mmol) and compound **8a** (0.0553 g, 0.1 mmol) were dissolved in 10 mL THF, and the solution was stirred at 0 ^{o}C for 30 min under an argon atmosphere. After that, potassium tertbutoxide (0.017 g, 0.15 mmol) dissolved in 5 mL THF were added dropwise slowly to above solution. The reaction mixture was stirred for another 30 min at room temperature, and then refluxed at 50 °C for 24 h. After cooling to room temperature, the reaction mixture was extracted with dichloromethane and washed with dilute aqueous HCl solution. The combined organic layers were dried over anhydrous $MgSO_4$, and then filtered. The filtrate was concentrated by rotary evaporation to give a red solid. The crude product was purified by column chromatography (silica gel; eluent: hexane: dichloromethane = 4:1) to afford **9a** (0.046 g, yield: 59%) as a red solid. ^{1}H NMR (400 MHz, $CDCl_3$, δ/ppm): 9.97 (s, 1H, ArH), 8.0-7.96 (m, 2H, ArH), 7.82-7.74 (m, 2H, ArH), 716-7.10 (m, 2H, ArH), 7.03-6.99 (m, 1H, ArH), 6.89-6.83 (m, 2H, CH), 2.82-2.80 (d, 2H, *J*=16.7 Hz, CH_2), 1.71 (br, 1H, CH), 1.32-1.27 (m, 24H, CH_2), 0.87-0.84 (m, 6H, CH_3). ^{13}C NMR (100 MHz, $CDCl_3$, δ/ppm): 152.53, 146.84, 142.86, 148.87, 139.23, 138.86, 136.97, 128.23, 127.96, 127.72, 126.46, 125.77, 124.88, 124.29, 119.89, 112.01, 110.12, 40.13, 34.74, 33.36, 33.27, 31.98, 30.04, 29.75, 29.62, 29.35, 26.62, 22.73, 14.12. Anal. Calcd for $C_{36}H_{42}N_2S_4Br_2$ (%): C, 54.68; H, 5.35; N, 3.54. Found (%): C, 54.97; H, 5.51; N, 3.22.

Monomer 9b. Compound **9b** was synthesized as a red solid according to the similar route as that for compound **9a** with a yield of 54%. ^{1}H NMR (400 MHz,

$CDCl_3$, δ/ppm): 8.84-8.33 (d, 1H, *J* = 9.1 Hz, ArH), 8.12-8.10 (d, 1H, *J* = 19.4 Hz, ArH), 7.13-7.12 (d, 1H, ArH), 7.07-7.06 (d, 1H, ArH), 7.97-6.93 (m, 1H, *J* = 39.9 Hz, ArH), 6.88-6.87 (d, 1H, *J* = 9.1 Hz, ArH), 6.84-6.80 (d, 1H, *J* = 39.9 Hz, ArH), 2.85-2.83 (d, 2H, *J* = 16.7 Hz, CH_2), 1.74 8-1.71 (m, 1H, CH), 1.35-1.26 (m, 24H, CH_2), 0.87-0.84 (m, 6H, CH_3). Anal. Calcd for $C_{40}H_{42}N_4Br_2S_5$ (%): C, 53.44; H, 4.71; N, 6.23. Found (%): C, 53.51; H, 4.36; N, 6.83.

Monomer 9c. Compound **9c** was synthesized as a red solid according to the similar route as that for compound **9a** with a yield of 54%. ^{1}H NMR (400 MHz, $CDCl_3$, δ/ppm): 9.02-8.99 (m, 1H, ArH), 8.93-8.90 (d, 1H, *J* = 28.9 Hz, ArH), 8.38-8.29 (m, 1H, ArH), 8.20-8.12 (m, 1H, ArH), 7.19-7.12 (m, 2H, ArH), 7.02-6.85 (m, 2H, ArH), 6.84-6.80 (d, 1H, *J* = 39.9 Hz, ArH), 2.99-2.91 (m, 2H, CH_2), 1.72 8-1.68 (m, 1H, CH), 1.41-1.25 (m, 24H, -CH_2-), 0.86-0.82 (m, 6H, CH_3). Anal. Calcd for $C_{40}H_{42}N_4Br_2S_6$ (%): C, 51.60; H, 4.55; N, 6.02. Found (%): C, 51.65; H, 5.14, N, 6.26.

Monomer 11. 4,8-Di(2,3-didecylthiophen-5-yl)-benzo[1,2-b:4,5-b']dithiophene (**10**) (1.91 g, 2.37 mmol) was dissolved in 50 mL of anhydrous THF under the protection of argon. The solution was then cooled to 0 °C, and a solution of *n*-BuLi (2.37 mL, 5.92 mmol, 2.5 M in hexane) was added dropwise slowly with stirring. After the addition was finished, the reaction mixture was warmed to ambient temperature and stirred for 2 hours. The reaction mixture was subsequently cooled to 0 °C and Sn(*n*-Bu)$_3$Cl (2.31 g, 7.11 mmol) was added in one portion. The reaction mixture was stirred at 0 °C for 30 minutes, and then warmed to room temperature for

another 8 h. After that, the reaction mixture was poured into water and extracted twice with dichloromethane. The combined organic layers were dried over $MgSO_4$, and the solvent was removed by rotary evaporation. The crude product was purified by column chromatography (silica gel; eluent: hexane: dichloromethane = 10:1) to afford compound **11** (1.51 g, yield 46%) as colorless liquid. ^{1}H NMR (400 MHz, $CDCl_3$, δ/ppm): 7.75 (s, 1H, ArH), 7.25 (s, 1H, ArH), 2.84-2.80 (t, 4H, ArH), 2.62-2.58 (t, 4H, ArH),1.75-1.71 (m, 4H, CH_2), 1.68-1.64 (m, 4H, CH_2), 1.61-1.56 (m, 12H, CH_2), 1.37-1.30 (m, 52H, CH_2), 1.20-1.16 (t, 12H, CH_2), 0.89-0.86 (m, 30H, CH_3). ^{13}C NMR (100 MHz, $CDCl_3$, δ/ppm): 143.03, 141.24, 139.71, 137.93, 137.17, 136.25, 131.89, 129.83, 122.26, 32.11, 32.04, 31.94, 31.07, 29.73, 29.59, 29.43, 29.20, 29.11, 29.04, 28.52, 28.18, 27.43, 22.82, 14.25, 13.85, 10.95. Anal. Calcd for $C_{74}H_{126}S_4Sn_4$ (%): C, 64.34; H, 9.19. Found (%): C, 64.75; H, 9.10.

PBDTT-TABT. Monomer **9a** (0.1862 g, 0.235mmol) and monomer **11** (0.3250 g, 0.235 mmol) were dissolved in 15 mL degassed toluene, and $Pd_2(dba)_3$ (5.67mg, 2% mmol) and P(*o*-tol)$_3$ (7.62 mg, 8% mmol) were added later under an argon atmosphere. The mixture was stirred at 110 °C for 24 h in a dark environment. After the reaction was finished, the mixture was cooled to room temperature and dropped into 500 mL methanol slowly to form a dark precipitate. The crude copolymer was collected by filtration, and then subjected to Soxhlet extraction successively with methanol, acetone, and hexane in turn to remove the oligomers and impurities. The remaining polymer was finally dissolved in chloroform and precipitated again from methanol to afford **PBDTT-TABT** (0.242g, yield 72%) as a dark solid. M_n = 27.0

KDa, M_w = 53.6 KDa, PDI=1.98. ^{1}H NMR (400 MHz, $CDCl_3$, δ/ppm): 8.71-6.87 (br, 13H, ArH, CH), 2.88-2.47 (br, 10H, CH_2), 2.03-0.86 (m, 91H, CH_3, CH_2). Anal. Calcd for $(C_{86}H_{114}N_2S_8)_n$ (%): C, 72.11; H, 8.02; N, 1.96. Found (%): C, 71.48; H, 7.99; N, 1.97.

PBDTT-TANT. Polymer **PBDTT-TANT** was synthesized as a dark solid according to the similar route as that for **PBDTT-TABT** with a yield of 69%. M_n = 15.9 KDa, M_w = 26.3 KDa, PDI = 1.6. ^{1}H NMR (400 MHz, $CDCl_3$, δ/ppm): 8.71-6.87 (br, 13H, ArH, CH), 2.88-2.47 (br, 10H, CH_2), 2.03-0.86 (m, 91H, CH_2, CH_3). Anal. Calcd for $(C_{90}H_{114}N_4S_9)_n$ (%): C, 70.17; H, 7.46; N, 3.64. Found (%): C, 70.14; H, 7.12; N, 3.60.

PBDTT-TSNT. Polymer **PBDTT-TSNT** was synthesized as a dark solid according to the similar route as that for **PBDTT-TABT** with a yield of 62%. M_n = 13.5 KDa, M_w = 24.5 KDa, PDI = 1.8. ^{1}H NMR (400 MHz, $CDCl_3$, δ/ppm): 7.80-6.99 (br, 13H, ArH, CH), 3.01-2.35 (br, 10H, CH_2), 2.03-0.83 (m, 91H, CH_2, CH_3). Anal. Calcd for $(C_{90}H_{114}N_4S_{10})_n$ (%): C, 68.74; H, 7.31; N, 3.56. Found (%): C, 68.38; H, 7.74; N, 3.99.

2.2 Characterization

^{1}H and ^{13}C NMR spectra were recorded on a Bruker Avance-400 spectrometer with dchloroform as a solvent and tetramethylsilane as an internal standard. The elemental analysis was performed on a Thermo Electron SPA Flash EA 1112 series analyzer. Molecular weights of the copolymers were determined by using a Waters 1515 GPC instrument with chloroform as the eluent and polystyrene as a standard.

Thermogravimetric analysis was conducted on a TA Instrument Model SDT Q600 simultaneous TGA/DSC analyzer at a heating rate of 10 °C min^{-1} and under a N_2 flow rate of 90 mL min^{-1}. UV-vis spectra were obtained on a carry 300 spectrophotometer. Cyclic voltammetry measurements were made on a CHI660 potentiostat/galvanostat electrochemical workstation at a scan rate of 50 mV s^{-1}, with a platinum wire counter electrode and an Ag/AgCl reference electrode in an anhydrous and nitrogen-saturated 0.1 mol L^{-1} acetonitrile solution of tetrabutylammonium perchlorate. The $CHCl_3$ solutions of the polymers were drop-coated on the platinum plate working electrodes. XRD patterns of the polymers were recorded on a Philips X-ray diffractometer operated in reflection geometry at 30 mA, 40 kV with Cu K_α radiation. AFM images were obtained by using a Bruker Inova atomic microscope at tapping mode. SCLC is described by $J=9\varepsilon_0\varepsilon_r\mu V^2/8L^3$, where J is the current density, L is the film thickness of active layer, μ is the hole or electron mobility, ε_r is the relative dielectric constant of the transport medium, ε_0 is the permittivity of free space (8.85×10^{-12} F m^{-1}), V is the internal voltage in the device and $V = V_{appl} - V_{bi} - V_a$, where V_{appl} is the applied voltage to the device, V_{bi} is the built-in voltage due to the relative work function difference of the two electrodes and V_a is the voltage drop due to contact resistance and series resistance across the electrodes.

2.3 Device fabrication

The device structure was ITO/PEDOT:PSS/copolymer:$PC_{71}BM$/Ca/Al. A glass substrate with a pre-patterned ITO (sheet resistance = 15 Ω sq^{-1}) was first ultrasonicated in detergent, deionized water, acetone, and isopropanol in turn, and

then modified by UV-ozone treatment for 20 min. After filtration through a 0.45 μm filter, PEDOT:PSS (Bay P VP AI 4083, Bayer AG) was spin-coated at 4000 rpm for 60 s to form a thickness of 35 nm thin layer on the cleaned ITO substrate, and baked on a hot plate at 140 °C for about 15 min. A blend film of copolymer:$PC_{71}BM$ (1:4 w/w) was prepared by spin-coating its mixed solvent of chlorobenzene (CB)/1,8-diiodoctane (DIO) (97:3, v:v) solution (concentration: 28 mg mL^{-1}) at 1500 r. p. m. for 60 s. A Ca layer (15 nm) and an Al layer (140 nm) were finally deposited in sequence under a vacuum of 2×10^{-6} Torr to form the negative electrode. Hole-only devices were fabricated similar to the PSCs with a structure of ITO/PEDOT:PSS/polymer:$PC_{71}BM$ (1:4)/MoO_3/Ag. 10 nm MoO_3 was evaporated onto the surface of the photoactive layer with or without surface modification before Al evaporation. All devices were fabricated in a nitrogen-filled glove box (< 0.1 ppm O_2 and H_2O). The thickness of films was measured using a Dektak 6 M surface profilometer. The device area was 0.04 cm^2. The I-V characterization of the devices was carried out on a computer-controlled Keithley 2400 Source Measurement system. The EQE values were tested with a Newport Model 77890 (Newport Co. Ltd.) during illumination with monochromatic light from a xenon lamp. A solar simulator was used as the light source, and the light intensity was monitored by using a standard Si solar cell. All fabrication and characterization processes, except for the EQE measurements, were conducted in a glove box.

3. Results and Discussion

3.1 Materials Synthesis and Characterization

The synthetic routes of monomers and the two-dimensional copolymers are shown in Scheme 1. The compounds **6a-6c** was synthesized by the Stille coupling reaction of the thienyltin derivatives (**4a** or **4b**) and BT or NT based dibromides (**5a** or **5b**). The other bromo side of **6a-6c** was terminated with 2-(tributylstannyl)thiophene by Stille coupling reaction again to afford compounds **7a-7c**. Using a Vilsmeier reaction, Compounds **7a-7c** was synthesized through formylation of the 2-position of thiophene unit in compounds **7a-7c**. After that, **7a-7c** reacted with (2,5-dibromothiophen-3-yl-methyl) phosphonic acid diethyl ester to give monomers **9a-9c**, using a Wittig-Horner reaction. Finally, the two-dimensional copolymers, PBDTT-T-DTBT, PBDTT-T-DTNT and PBDTT-T-DTSNT, were prepared by Stille coupling polymerization in good yields using $Pd_2(dba)_3/P(o\text{-tol})_3$ as the catalyst system. The molecular structures of the intermediates and copolymers were confirmed by ^1H NMR spectroscopy, ^{13}C NMR spectroscopy and elemental analysis. All the copolymers show good solubility in common organic solvents, such as chloroform, toluene, chlorobenzene, dichlorobenzene. The molecular weights (M_w and M_n) and polydispersity indices (PDIs) of the copolymers were determined by gel permeation chromatography (GPC) analysis with a polystyrene standard calibration. PBDTT-TANT and PBDTT-TSNT have comparable number-average molecular weights (M_n) with 15.9 KDa and 13.5 KDa, respectively. However, PBDTT-TABT exhibits relatively higher M_n of 27.0 KDa, which might be attributed to the decreased steric hindrance of dibromothiophene monomer (**9a**) with BT containing side chain. The thermal stabilities of the copolymers were evaluated by thermogravimetric (TGA)

analysis. As shown in Fig. 2a, the decomposition temperatures (T_d, 5% weight loss) of PBDTT-TABT, PBDTT-TANT and PBDTT-TSNT were measured to be 416 ^{o}C, 416 ^{o}C and 360 ^{o}C, respectively. The results indicated that using NT instead of BT could not significantly increase the thermal properties of BDT-T based copolymers while the alkylthio flexile side chains would reduce the thermal stability of the resulting copolymers compared to the alkyl side chains. In any event, the thermal stability of the three copolymers is good enough for their device fabrications and evaluations. The differential scanning calorimetry (DSC) curves of PBDTT-TABT, PBDTT-TANT and PBDTT-TSNT are also shown in Fig. 2b. No glass transition was observed for all these copolymers from their DSC heating and cooling traces in the range of room temperature to 200 ^{o}C. The molecular weights and the thermal analysis data are listed in Table 1.

2.2 Optical Properties

The UV-vis absorption spectra of the two-dimensional copolymers in chloroform solution and thin film are shown in Fig. 3. The corresponding absorption data of the copolymers are summarized in Table 2. As shown in Fig. 3a, these copolymers show two distinct absorption characteristics in solution. The absorption band in the high energy region is owned to π-π* transition of polymer backbones, and the other in the lower energy region comes from the intramolecular charge transfer (ICT) between the donor units of main chains and the acceptor units of side chains. The low-energy peaks of PBDTT-TABT, PBDTT-TANT and PBDTT-TSNT in $CHCl_3$ were located at about 490 nm, 492 nm and 495 nm**,** respectively. PBDTT-TANT and PBDTT-TSNT

with NT side chains show red-shifted absorption in contrast to that of PBDTT-TABT with BT side chains. The reason is attributed to the boosted ICT properties, originating from the stronger electron-withdrawing ability of NT unit. Compared with PBDTT-TANT, the absorption is red-shifted for PBDTT-TSNT in solution. This is probably attributed to that the introduced alkylthio moiety shows an electron-donating ability, which can increase the ICT effect between the main chain and the side chain to a certain extent. As shown in Fig. 2, similar behavior was observed from the absorption spectra of these copolymers as thin solid films. Relative to their counterparts in the solution state, the absorption shapes became broader in the wavelength range of 300-800 nm, and the peaks showed slight red-shifts for all the three copolymers. The reason could be explained by the enhanced aggregation and strengthened interchain interactions between the conjugated backbones in the solid state, which could facilitate charge transportation in PSCs.[24] The optical bandgaps of PBDTT-TABT, PBDTT-TANT and PBDTT-TSNT were determined from the absorption onsets of the corresponding copolymer films to be 1.98 eV, 1.87 eV and 1.85 eV, respectively. PBDTT-TANT and PBDTT-TSNT showed the smaller bandgaps than that of PBDTT-TANT, which was ascribed to the stronger electron-withdrawing ability of NT unit, generating an enhanced ICT effect between the main chain and the side chain. The smallest bandgap of PBDTT-TANT would be expected to harvest more sunlight to increase the J_{sc} value in its PSCs.

3.3 Electrochemical Properties

The energy levels are important parameters to select appropriate acceptors in BHJ

PSCs.[1d] Thus, cyclic voltammetry (CV) was employed to investigate the redox behaviors of the copolymers and determine their energy levels. The CV experiments were performed in a three-electrode cell, using 0.10 M tetrabutylammonium perchlorate (n-Bu_4NClO_4) as the supporting electrolyte in anhydrous acetonitrile. A platinum plate coated with a thin film of the studied copolymer, a platinum wire and Ag/AgCl (0.1 M) were used as the work, counter and reference electrodes, respectively. The energy level of the Ag/AgCl reference electrode was calibrated against the Fc/Fc^+ system to be 4.34 eV by using the previous methods.[19] As shown in Fig. 3, the onset oxidation potentials of PBDTT-TABT, PBDTT-TANT and PBDTT-TSNT were located at 1.11 V, 1.03 V and 1.07 V, leading to the corresponding HOMO levels of -5.45 eV, -5.37 eV and -5.41 eV, respectively. The low-lying HOMO levels of these copolymers implied their enhanced chemical stability in ambient conditions. Furthermore, the deepened HOMO energy levels could be helpful to obtain the relatively high V_{oc}s of their PSCs because V_{oc} is proportional to the energy level difference between HOMO of the donor and LUMO of the acceptor.[20] Compared to PBDTT-TANT, PBDTT-TSNT showed a lower HOMO energy level, which could be attributed to the effect of alkylthio modification.[6a,14] On the other hand, the lowest unoccupied molecular orbital (LUMO) energy levels of PBDTT-TABT, PBDTT-TANT and PBDTT-TSNT were calculated to be -3.31 eV, -3.39 eV and -3.44 eV, respectively. As shown in Fig. 4b, the LUMO gaps of 0.56-0.69 eV between the copolymers and $PC_{71}BM$ would afford an enough driving force to facilitate an efficient exciton dissociation at the D-A interface, thereby ensuring energetically

favorable electron transfer to overcome the binding energy of the intrachain exciton.[21] The corresponding electrochemical data of these copolymers are summarized in Table 2.

3.4 Theoretical Calculations

To evaluate the side chain effect on the molecular architectures and electronic properties of the resulting copolymers, Density Functional Theory (DFT) simulations were performed on the model monomers with three repeated donor-acceptor units to verify stationary points as stable states for the optimized conformations and single-point energies, at the B3LYP/6-31G(d) level.[22] To simplify the calculations, long alkyl chains were replaced by the methyl group because they did not significantly affect the equilibrium geometries and electronic properties.[22] The HOMO and LUMO wave functions of the model compounds are shown in Fig. 5. These copolymers show similar distributions for both the HOMO and LUMO. As shown in Fig. 5, the localization of HOMO was distributed in the electron-rich skeleton of the polymer backbone while the LUMO was mainly located on the electron-deficient BT or NT containing side chains. Compared to HOMOs, HOMO-1 orbitals moved from the middle part to the side parts even distributing on the side chains to some extent, which implied that internal charge transfer was possible in these two-dimensional conjugation systems. A similar transfer trend is observed from the LUMO to LUMO+1. The results indicated that the significant charge-transfer character occurred between the BDT-T main chains and conjugated side chains, which was consistent with the observed strong low-energy absorption band in Fig. 2. The

HOMO and LUMO energy levels of PBDTT-TABT, PBDTT-TANT and PBDTT-TSNT trimers were calculated to be -4.86/-2.66 eV, -4.80/-2.91 eV and -4.83/-2.98 eV, respectively. The bandgaps were then determined to be 2.20, 1.89 and 1.85 eV. Obviously, the trend of simulation results were agreed well with those obtained from CV and UV-vis measurements.

3.5 X-ray Diffraction Analysis

To investigate an insight of the molecular stacking of the two-dimensional copolymers, X-ray diffraction (XRD) patterns were measured for PBDTT-TABT, PBDTT-TANT and PBDTT-TSNT. As shown in Fig. 6, XRD patterns of these copolymers exhibited two types of diffraction peaks. In the small angle region, clear (100) peaks were located at 2θ of 4.00°, 3.73° and 3.82° for PBDTT-TABT, PBDTT-TANT and PBDTT-TSNT，corresponding to the lamellar packing with a *d*-spacing (d_{100}) of 22.06 Å, 23.66Å and 23.10 Å. The second peaks (010) in the wide angle region reflected the π–π stacking distances between the polymer backbones, which were located at 2θ of 21.95°, 22.22° and 21.79° for PBDTT-TABT, PBDTT-TANT and PBDTT-TSNT, corresponding to a π-π stacking distance (d_{010}) of 4.04 Å, 4.00 Å and 4.07 Å, respectively. Because the bulk size of NT side chain is larger than that of BT side chain, PBDTT-TANT possesses a longer lamellar packing distance than PBDTT-TABT. After introducing alkythio group instead of alkyl group, the flexibility of alkyl chain would be increased, confirming a little decrease of lamellar packing distance obtained from PBDTT-TSNT film. On the other hand, PBDTT-TANT shows the shorter π-π stacking distance than PBDTT-TABT, which can

be attributed to the enhanced interaction of conjugated polymer chains by choosing the NT unit with a stronger electron-withdrawing ability. Surprisingly, after introducing alkylthio unit instead of alkyl unit, the π-π stacking distance of PBDTT-TSNT becomes larger even than PBDTT-TABT with BT side chains. The result indicated that the effect of alkylthio modification *via* S-S interaction on the ordered molecular stacking would not work in this type of two-dimensional system, however, the positive influence of alkylthio modification is commonly observed in linear conjugated polymer donor materials.[6a,14] Through the comprehensive consideration of above XRD results, PBDTT-TANT shows the best stacking properties, which can be expected to gain the highest carrier mobility in PSCs.

3.6 Photovoltaic Properties

To study the photovoltaic properties of the resulting copolymers, PSCs with a device structure ITO/PEDOT:PSS/copolymer:$PC_{71}BM$/Ca/Al were fabricated and evaluated. The active layers were spin-coated from chlorobenzene (CB) solution of the donor and acceptor materials. The optimized condition of device fabrication was obtained by varying polymer:$PC_{71}BM$ weight ratios, active layer thicknesses, and solvent additives. The best photovoltaic properties were obtained with the blend ratio of 1:4 with 3% (v/v) 1,8-diiodooctane (DIO) as the solvent additive for all the three copolymers based PSCs. Fig. 7 shows the current density-voltage (J-V) and external quantum efficiency (EQE) curves of optimized devices. The related photovoltaic parameters are summarized in Table 3.

As shown in Fig. 7a, the PBDTT-TABT:$PC_{71}BM$ device showed a PCE of 4.60%,

with a V_{oc} of 1.00 V, a J_{sc} of 9.64 mA cm^{-2} and an FF of 47.5%, which was superior to that of PSC device based on PTG1 with a similar molecular structure.[12,13] Under the same conditions, PBDTT-TANT device exhibited a higher PCE of 5.65% with a V_{oc} of 0.98 V, a J_{sc} of 10.00 mA cm^{-2} and an FF of 58.0%. But a decreased PCE of 4.01% with a V_{oc} of 0.99 V, a J_{sc} of 8.93 mA cm^{-2} and an FF of 45.3% was obtained for PBDTT-TSNT device. Since the V_{oc} is related to the HOMO of donor and LUMO of acceptor energy offset,[2] the obtained high V_{oc} values of these devices should result from the low-lying HOMO levels of the polymer donors as determined in CV measurements. The highest V_{oc} value of 1.00 V from PBDTT-TABT device could be due to its deepest HOMO level as compared to those of PBDTT-TANT and PBDTT-TSNT. Except for the decreased V_{oc}, the simultaneously improvements of J_{sc} and FF guaranteed achieving the highest PCE of 5.65% for PBDTT-TANT device. The increased J_{sc} could be confirmed by EQE measurements. As shown in Fig. 7b, the EQE response of these devices covered a broad range from 300 to 750 nm, which corresponded to the absorptions of both the copolymer donor and the fullerene acceptor. The maximum EQE values in the range of 450-650 nm reached about 63%, 68% and 59% for PBDTT-TABT, PBDTT-TANT and PBDTT-TSNT devices, respectively. The EQE values are in good agreement with the J_{sc} values from J-V measurements.

Solvent vapor annealing (SVA) using some polar solvents before the deposition of cathode is an effective strategy to optimize the performance of PSCs *via* the formation of more favorable phase separation.[23] Thus, we employed tetrahydrofuran (THF)-SVA

to further improve the PCEs of the PSCs based on these two-dimensional copolymers. SVA treatment was performed in a glass Petri dish at room temperature in a glove box. A 30 mm Petri dish was first injected about 2 mL THF and then closed for one minute to ensure the THF vapor saturate the whole chamber. Then the active film was transferred to the Petri dish and kept for 30 s before it was removed out. From Fig. 7a and Table 3, in comparison with the performance of the PSCs without SVA treatments, the PCEs of the three copolymers based PSCs increased greatly after a SVA process. The PCEs increased from 4.60% to 6.74% for PBDTT-TABT device, from 5.65% to 8.04% for PBDTT-TANT device, and from 4.01% to 6.00% for PBDTT-TSNT device, respectively. All the PSCs showed the improvement of PCE values more than 40%, which indicated that the THF-SVA treatment was an effective method to optimize the photovoltaic property of this polymer donor system. To our knowledge, the PCE of 8.04% is the highest value of this type of two-dimensional copolymers with D-D polymer backbones and D-A conjugated side chains. It is clearly that the V_{oc}s of these devices decreased a little after the SVA treatments, which is also observed in the previous reported work.[23] Despite of this, the J_{sc} and FF showed a significant improvement, giving rise to a large increase of PCEs for all the devices by SVA treatments. From the Table 3, the J_{sc} values were improved from 9.64, 10.00 and 8.93 mA cm^{-2} to 11.12, 13.06 and 10.25 mA cm^{-2} for PBDTT-TABT, PBDTT-TANT and PBDTT-TSNT devices, respectively. The EQE spectra were also measured to verify the elevation of J_{sc}s, which are plotted in Fig. 7b. The EQE values of all the devices with SVA treatments exhibited higher responses than those without SVA treatments.

The largest increase of PBDTT-TANT device up to 78% supported its highest J_{sc} of 13.06 mA cm^{-2}. The enhanced device performance after SVA treatments, especially in J_{sc} and FF, is also confirmed by measuring the series resistance (R_s) and shunt resistance (R_{sh}). In fact, a decrease in R_s and/or an increase in R_{sh} are essential to achieving high J_{sc} and FF.[25] For all the devices using SVA treatments, the R_s and R_{sh} showed the same variation trends. Take PBDTT-TANT device as an example, the R_s decreased from 16.0 Ω cm^2 to 10.8 Ω cm^2, while the R_{sh} increased from 549.6 Ω cm^2 to 629.2 Ω cm^2. The lowest R_s and the highest R_{sh} of PBDTT-TANT device indicated that the best ohmic contact was achieved at the interfaces of active layer/cathode, which is beneficial for charge transport and extraction.

3.7 Hole Mobility

To further understand the origin of enhanced J_{sc} with SVA treatments, the hole-only devices with a configuration of ITO/PEDOT:PSS/copolymer:$PC_{71}BM$ (1:4)/MoO_3/Ag were fabricated in order to determine the hole mobilities of three copolymers based blend films by space-charge-limited current (SCLC) method.[26] The J-V curves of the hole-only devices are shown in Fig. 8, and the corresponding data are summarized in Table 4. Without the SVA treatments, the hole mobilities were measured to be 2.40 × 10^{-4} cm^2 V^{-1} s^{-1}, 2.93×10^{-4} cm^2 V^{-1} s^{-1} and 1.33×10^{-4} cm^2 V^{-1} s^{-1} for PBDTT-TABT, PBDTT-TANT and PBDTT-TSNT blend films, respectively. PBDTT-TANT blend film exhibited the highest hole mobility, which could be attributed to its best crystallinity and stacking property among these copolymers, as discussed in the XRD section. This also supports the highest J_{sc} value obtained for the PBDTT-TANT device.

On the other hand, PBDTT-TABT, PBDTT-TANT and PBDTT-TSNT blend films with the SVA treatments exhibited relatively higher hole mobilities of 3.28×10^{-4} cm^2 V^{-1} s^{-1}, 3.94×10^{-4} cm^2 V^{-1} s^{-1} and 2.18×10^{-4} cm^2 V^{-1} s^{-1}. In comparison with their counterparts without SVA treatments, the blend films showed 1.37, 1.34 and 1.64 fold increases for PBDTT-TABT, PBDTT-TANT and PBDTT-TSNT, respectively. Therefore, the THF-SVA treatment of active layers could effectively improve the carrier transport property, and thereby afford the higher J_{sc} values and PCEs of the related PSCs.

3.8 Morphology Study

To investigate the phase separation of the active blend films and the SVA effect on the device performance, atomic force microscopy (AFM) was used to study the surface morphology of these blend layers. The AFM topography and phase images are shown in Fig. 9. As shown in Fig. 9, each polymer blend showed the different surface morphology with or without THF-SVA. Without SVA treatments, all the three blend films had the smooth surfaces with the root-mean-square (RMS) surface roughness values of 0.80 nm, 0.60 nm and 0.79 nm for PBDTT-TABT, PBDTT-TANT and PBDTT-TSNT, indicating all of the copolymer donors have a good miscibility with $PC_{71}BM$. After the THF-SVA treatment for 30 s, the blend films were more phase separated, featured with larger surface aggregates and more notable phase domain. The RMS values of the active layers increased to 1.63 nm, 1.08 nm and 1.76 nm for PBDTT-TABT, PBDTT-TANT and PBDTT-TSNT, respectively. The increased roughness values caused by SVA treatments are similar to the results reported by other

groups.[23] Apparently, the THF-SVA process provided a driving force to facilitate domain grow, forming a more distinct bi-continuous network of the donor and acceptor-rich domains.[23,27] PBDTT-TANT based blend surface after the THF-SVA treatment exhibited the best interpenetrating networks with defined and distinct nanoscale phase separation, which was beneficial for charge transport, resulting in high J_{sc} and FF of its PSCs.

4. Conclusions

In summary, a series of new two-dimensional BDT-T copolymers, PBDTT-TABT, PBDTT-TANT and PBDTT-TSNT, with conjugated BT or NT side chains were successfully synthesized and characterized for efficient PSCs. Compared with BT unit, NT unit has a stronger electron-withdrawing ability and an extended conjugation, which induced the stronger ICT effect between the polymeric backbone and the conjugated side chain for NT containing copolymers. Thus, PBDTT-TANT and PBDTT-TSNT showed the lower bandgaps and the more red-shifted absorption than those of PBDTT-TABT. The alkylthio modification effect of side chains was also investigated, and the results indicated that it only showed a positive role in lowering the HOMO energy level while a negative role in elevating carrier mobility and molecular stacking property in this type of polymeric system. BHJ PSCs were fabricated with the three copolymers as the donor materials to evaluate their photovoltaic performance. These devices exhibited PCEs of 4.60% for PBDTT-TABT, 5.65% for PBDTT-TANT and 4.01% for PBDTT-TSNT, respectively. Despite of V_{oc}, the enhanced J_{sc}, FF and PCE were achieved for PBDTT-TANT device, which was

attributed to its red-shifted absorption, improved stacking property and well-defined phase separation of the related blend film. When using the THF-SVA treatment, the J_{sc}s and FFs of all the devices were improved significantly, give rising to much higher PCEs. The THF-SVA process would provide a driving force to facilitate domain grow to form a more distinct bi-continuous network of the donor and acceptor-rich domains. PBDTT-TANT device showed the highest PCE of 8.04%, which is the best efficiency for this type of two-dimensional copolymers with D-D polymer backbones and D-A conjugated side chains. Our design strategy would give an instructive meaning in developing high performance two-dimensional polymer donors in PSCs.

Acknowledgments

This work was supported by the NSFC (51573107, 21432005), the 863 Project (No: 2013AA031901), the Youth Science and Technology Foundation of Sichuan Province (2013JQ0032), the Foundation of State Key Laboratory of Polymer Materials Engineering (sklpme2014-3-05, sklpme2015-2-01), and the Fundamental Research Funds for the Central Universities (2012SCU04B01, YJ2011025). We also appreciate the comprehensive training platform of specialized laboratory, college of chemistry, Sichuan University, for the NMR, elemental analysis, DSC, TGA measurements.

References

1 (a) Z. C. He, C. M. Zhong, S. J. Su, M. Xu, H. B. Wu and Y. Cao, *Nat. Photonics,* 2012, **6**, 593; (b) S. H. Park, A. Roy, S. Beaupré, S. Cho, N. Coates, J. S. Moon, D. Moses, M. Leclerc, K. Lee and A. J. Heeger, *Nat. Photonics,* 2009, **3**, 297; (c) Y. J. Cheng, S. H. Yang and C. S. Hsu, *Chem. Rev.,* 2009, **109**, 5868; (d) Y. F. Li, *Acc.*

Chem. Res., 2012, **45**, 723.

2 (a) Q. Peng, K. Park, T. Lin, M. Durstock and L. M. Dai, *J. Phys. Chem. B,* 2008, **112**, 2801; (b) J. Warnan, C. Cabanetos, R. Bude, A. E. Labban, L. Li and P. M. Beaujuge, *Chem. Mater.,* 2014, **26**, 2829.

3 S. Liu, P. You, J. Li, J. Li, C. S. Lee, B. S. Ong, C. Surya and F. Yan, *Energy Environ. Sci.,* 2015, **8**, 1463.

4 (a) Q. Peng, X. J. Liu, D. Su, G. W. Fu, J. Xu and L. M. Dai, *Adv. Mater.,* 2011, **23**, 4554; (b) X. Guo, N. Zhou, S. J. Lou, J. Smith, D. B. Tice, J. W. Hennek, R. P. Ortiz, J. T. L. Navarrete, S. Li, J. Strzalka, L. X. Chen, R. P. H. Chang, A. Facchetti and T. J. Marks, *Nat. Photonics,* 2013, **7**, 825.

5 G. Yu, J. Gao, J. C. Hummelen, F. Wudi and A. J. Heeger, *Science,* 1995, **270**, 1789.

6 (a) K. Li, Z. J. Li, K. Feng, X. P. Xu, L. Y. Wang and Q. Peng, *J. Am. Chem. Soc.,* 2013, **135**, 13549; (b) Y. Liu, J. Zhao, Z. Li, C. Mu, W. Ma, H. Hu, K. Jiang, H. Lin, H. Ade and H. Yan, *Nat. Commun.,* 2014, **5**, 5293; (c) L. Nian, W. Q. Zhang, N. Zhu, L. Liu, Z. Q Xie, H. B. Wu, F. Wurthner and Y. G. Ma, *J. Am. Chem. Soc.,* 2015, **137**, 6995; (d) L. J. Huo, T. Liu, X. B. Sun, Y. H. Cai, A. J. Heeger and Y. M. Sun, *Adv. Mater.,* 2015, **27**, 2938.

7. Y. Y. Lai, Y. J. Cheng and C. S. Hsu, *Energy Environ.Sci.,* 2014, **7**, 1866.

8 (a) J. H. Hou, Z. A. Tan, Y. Yan, Y. J. He, C. H. Yang and Y. F. Li, *J. Am. Chem. Soc.,* 2006, **128**, 4911; (b) F. Huang, K. S. Chen, H. L. Yip, S. K. Hau, O. Acton, Y. Zhang, J. D. Luo and A. K. Y. Jen, *J. Am. Chem. Soc.*, 2009, **131**, 13886; (c) L. J. Huo, J. H. Hou, S. Q. Zhang, H. Y. Chen and Y. Yang. *Angew. Chem. Int. Ed.,* 2010, **49**, 1500; (d)

Z. J. Gu, P. Shen, S. W. Tsang, Y. Tao, B. Zhao, P. Tang, Y. J. Nie, Y. Fang and S. T. Tan, *Chem.Commun.,* **2011**, *47*, 9381; (e) Q. Peng, S. L. Lim, I. H. K. Wong, J. Xu and Z. K. Chen, *Chem. Eur. J.,* 2012, **18**, 12140; (f) K. Feng, X. P. Xu, Z. J. Li, Y. Li, K. Li, T. Yu and Q. Peng, *Chem. Commun.,* 2015, **51**, 6290; (g) Y. Li, X. P. Xu, Z. J. Li, T. Yu and Q. Peng, *Sci. China. Chem.,* 2015, **58**, 276; (h) Z. G. Zhang and Y. F. Li, *Sci. China. Chem.,* 2015, **58**, 192.

9 (a) J. H. Hou, L. J. Huo, C. He, C. H. Yang and Y. F. Li, *Macromolecules*, 2006, **39**, 594; (b) Y. P. Zou, W. P. Wu, G. Y. Sang, Y. Yang, Y. Q. Liu and Y. F. Li, *Macromolecules*, 2007, **40**, 7231; (c) E. J. Zhou, Z. A. Tan, Y. Yang, L. J. Hou, Y. P. Zou, C. H. Yang and Y. F. Li, *Macromolecules*, 2007, **40**, 1831.

10 (a) W. W. Li, Y. Han, Y. L. Chen, C. H. Li, B. S. Li and Z. S. Bo, *Macromol. Chem. Phys.,* 2010, **211**, 948; (b) G. Y. Sang, Y. P. Zou and Y. F. Li, *J. Phys. Chem. C,* 2008, **112**, 12058; (c) Y. T. Chang, S. L. Hsu, M. H. Su and K. H. Wei, *Adv. Funct. Mater.,* 2007, **17**, 3326; (d) Y. T. Chang, S. L. Hsu, M. H. Su and K. H. Wei, *Adv. Mater.,* 2009, **21**, 2093.

11 (a) L. J. Huo, S. Q. Zhang, X. Guo, F. Xu, Y. F. Li and J. H. Hou, *Angew. Chem. Int. Ed.,* 2011, **50**, 9697; (b) L. T. Dou, J. Gao, E. Richard, J. B. You, C. C. Chen, K. C. Cha, Y. J. He, G. Li and Y. Yang, *J. Am. Chem. Soc.,* 2012, **134**, 10071; (c) L. Ye, S. Q. Zhang, L. J. Huo, M. J. Zhang and J. H. Hou. *Acc. Chem. Res.,* 2014, **47**, 1595.

12 C. W. Wang, B. Zhao, Z. C. Cao, P. Shen, Z. Tan, X. L. Li and S. T. Tan, *Chem. Commun.,* 2013, **49**, 3857.

13 P. Shen, H. J. Bin, L. Xiao and Y. F. Li, *Macromolecules,* 2013, **46**, 9575.

14 M. Wang, X. W. Hu, P. Liu, W. Li, X. Gong, F. Huang and Y. Cao, *J. Am. Chem. Soc.,* 2011, **133**, 9638.

15 (a) C. H. Cui, W. Y. Wong and Y. F. Li, *Energy Environ. Sci.,* 2014, **7**, 2276; (b) L.Ye, S. Q. Zhang, W. Zhao, H. Yao and J. H. Hou, *Chem. Mater.,* 2014, **26**, 3603; (c) H. F. Yao, L. Ye, B. H. Fan, L. J. Huo and J. H. Hou. *Sci. China Mater.,* 2015, **58**, 213.

16 X. L. Shi, J. J. Chang and C. Y. Chi, *Chem. Commun.,*2013, **49**, 7135.

17 Q. Peng. J. Xu and W. X. Zheng, *J. Polym. Sci. Part A: Polym. Chem.,* 2009, **47**, 3399.

18 Z. J. Gu, L. J. Deng, H. Luo, X. Guo, H. H. Li, Z. C. Cao, X. S. Liu, X. W. Li, H. Y. Huang, Y. Z. Tan, Y. Pei and S. T. Tan, *J. Polym. Sci. Part A: Polym. Chem.,* 2012, **50**, 3848.

19 (a) Y. F. Li, Y. Cao, J. Gao, D. L. Wang, G. Yu and A. J. Heeger, *Synth. Met.,* 1999, **99**, 243; (b) Q. Peng, Z. Y. Lu, Y. Huang, M. G. Xie, S. H. Han, J. B. Peng and Y. Cao, *Macromolecules,* 2004, **37**, 260; (c) X. P. Xu, Y. L. Wu, J. F. Fang, Z. J. Li, Z. G. Wang, Y. Li and Q. Peng, *Chem. Eur. J.,* 2014, **20**, 13259.

20 M. C. Scharber, D. Mühlbacher, M. Koppe, P. Denk, C. Waldauf, A. J. Heeger and C. J. Brabec, *Adv. Mater.,* 2006, **18**, 789.

21 C. J. Brabec, C. Winder, N. S. Sariciftci, J. C. Hummelen, A. Dhanabalan, P. A. van Hal and R. A. J. Janssen, *Adv. Funct. Mater.,* 2002, **12**, 709.

22 Z. Zeng, Y. Li, J. F. Deng, Q. Huang and Q. Peng, *J. Mater. Chem. A*, 2014, **2**, 653.

23 (a) C. D. Wessendorf, G. L. Schulz, A. Mishra, P. Kar, I. Ata, M. Weidelener, M. Urdanpilleta, J. Hanisch, E. Mena-Osteritz, M. Lindén, E. Ahlswede and P. Bäuerle,

Adv. Energy Mater., 2014, **4**, 1400266. (b) K. Sun, Z. Xiao, E. Hanssen, M. F. G. Klein, H. H. Dam, M. Pfaff, D. Gerthsen, W. W. H. Wong and D. J. Jones, *J. Mater. Chem. A*, 2014, **2**, 9048.

24 Q. Peng, Y. Y. Fu, X. J. Liu, J. Xu and Z. Y. Xie, *Polym. Chem.,* 2012, **3**, 2933.

25 (a) S. Liu, G. Zhang, J. Lu, J. Jia, W. Li, F. Huang, Y. Cao, *J. Mater. Chem. C* **2015**, 3, 4372. (b) W. Yu, L. Huang, D. Yang, P. Fu, L. Zhou, J. Zhang, C. Li, *J. Mater. Chem. A* **2015**, 3, 10660.

26 (a) X. P. Xu, Y. L. Wu, J. F. Fang, Z. J. Li, Z. G. Wang, Y. Li and Q. Peng, *Chem. Eur. J.* **2014**, *20*, 13259. (b) X. P. Xu, K. Li, Z. J. Li, Y. Li, Z. G. Wang and Q. Peng, *Polym. Chem.* **2015**, 6, 2337.

27 G. Wei, S. Wang, K. Sun, M. E. Thompson, S. R. Forrest, *Adv. Energy. Mater.* **2011**, 1, 184.

Legends for Schemes, Figures and Tables

Fig. 1 Design strategy and molecular structures of the two-dimensional copolymers in this work.

Scheme 1 Synthetic routes of the monomers and the two-dimensional copolymers.

Fig. 2 (a) Thermogravimetric (TGA) curves of the copolymers. (b) Differential scanning calorimetry (DSC) curves of the copolymers

Fig. 3 UV-vis absorption spectra of the copolymers in $CHCl_3$ solution (a) and in thin film (b).

Fig. 4 (a) Cyclic voltammograms of the copolymer films. (b) HOMO and LUMO energy levels of the copolymers and $PC_{71}BM$.

Fig. 5 Molecular structures and optimized molecular orbital surfaces of the LUMO+1, LUMO, HOMO, and HOMO-1 of the copolymers.

Fig. 6 X-ray diffraction patterns of the copolymers films on silicon wafers.

Fig. 7 (a) J-V curves of the PSCs under AM 1.5 G illumination with or without the SVA treatments. (b) EQE curves of the PSCs with or without the SVA treatments.

Fig. 8 $J^{1/2}$-V plots for polymer:$PC_{71}BM$ (1:4) devices with or without the SVA treatments.

Fig. 9 AFM images of $PC_{71}BM$ blended with PBDTT-TABT, PBDTT-TANT and PBDTT-TSNT without the SVA (a, b, c) measurements and with the SVA (d, e, f) treatments, respectively.

Table 1 Polymerization results and thermal properties of the copolymers.

Table 2 Optical properties and electrochemical data of the copolymers.

Table 3 Photovoltaic parameters of the PSCs under AM 1.5G illumination (100 mW cm^{-2}).

Table 4 Hole mobility of copolymer:$PC_{71}BM$ blends with or without the SVA treatments.

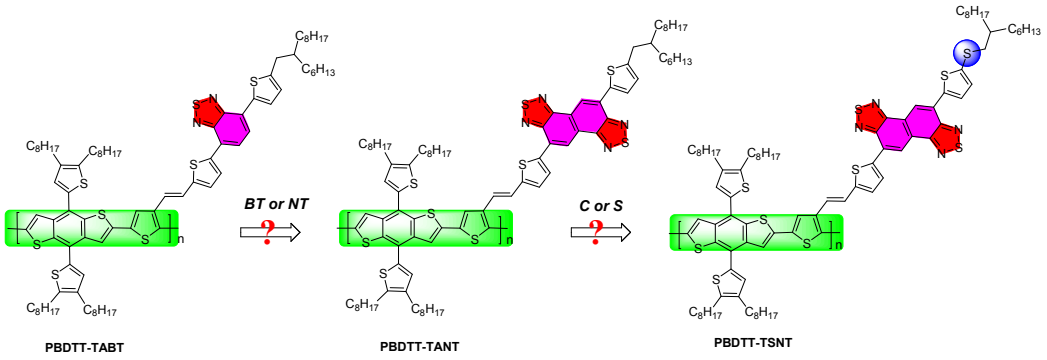

Fig. 1 Design strategy and molecular structures of the two-dimensional copolymers in this work.

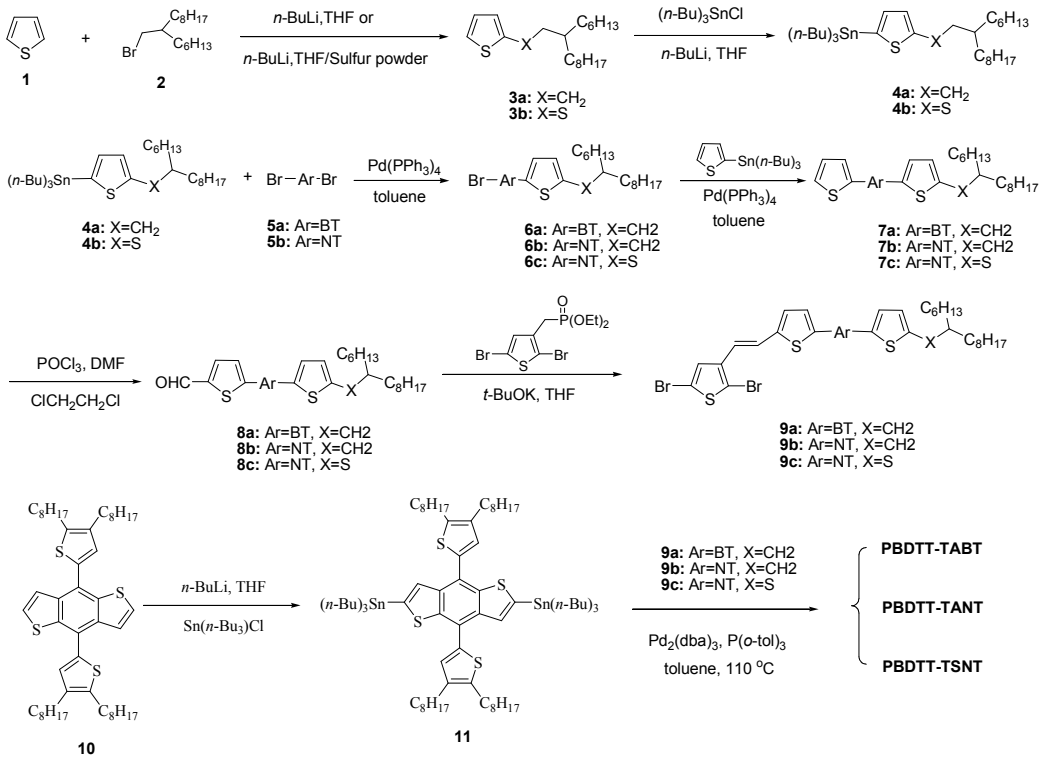

Scheme 1 Synthetic routes of the monomers and the copolymers.

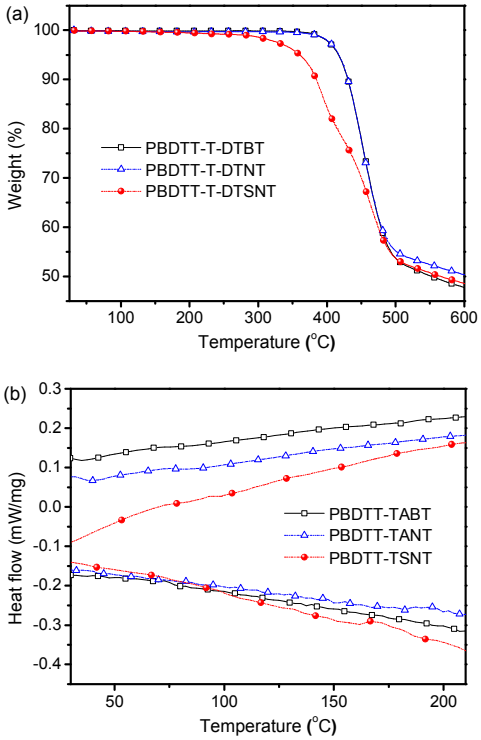

Fig. 2 (a) Thermogravimetric (TGA) curves of the copolymers. (b) Differential scanning calorimetry (DSC) curves of the copolymers

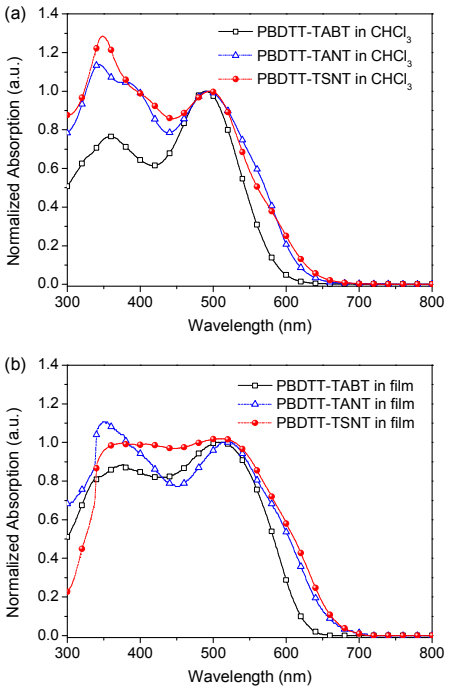

Fig. 3 UV-vis absorption spectra of the copolymers in $CHCl_3$ solution (a) and in thin film (b).

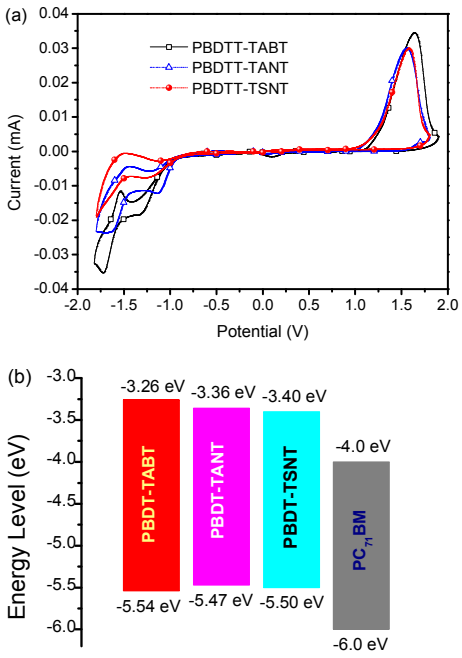

Fig. 4 (a) Cyclic voltammograms of the copolymer films. (b) HOMO and LUMO energy levels of the copolymers and $PC_{71}BM$.

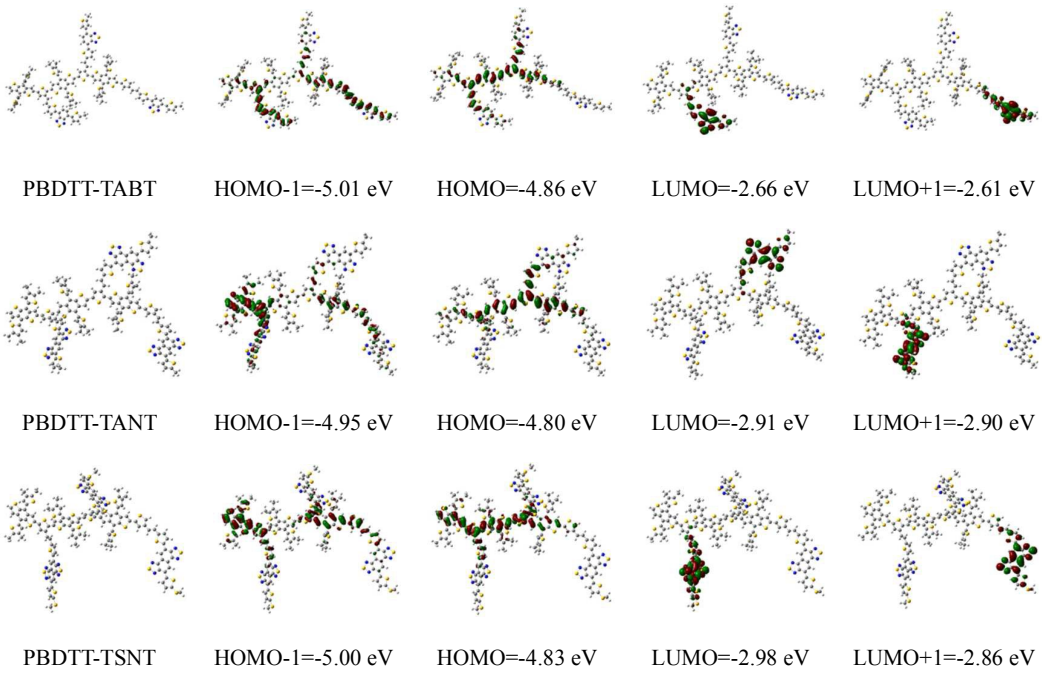

Fig. 5 Molecular structures and optimized molecular orbital surfaces of the LUMO+1, LUMO, HOMO, and HOMO-1 of the copolymers.

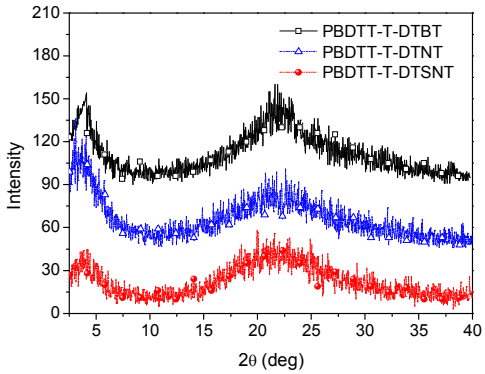

Fig. 6 X-ray diffraction patterns of the copolymers films on silicon wafers.

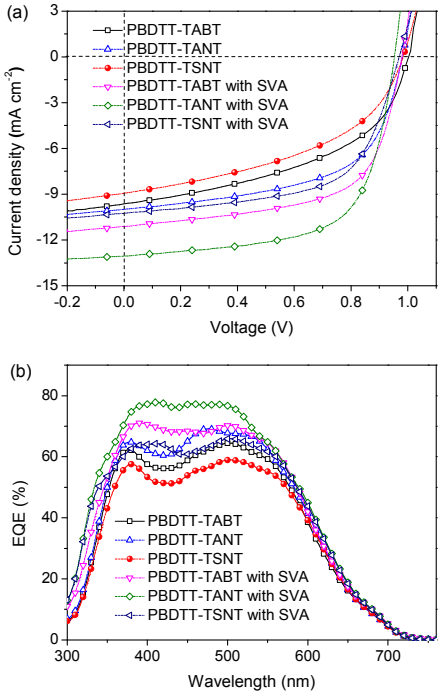

Fig. 7 (a) J-V curves of the PSCs under AM 1.5 G illumination with or without the SVA treatments. (b) EQE curves of the PSCs with or without the SVA treatments.

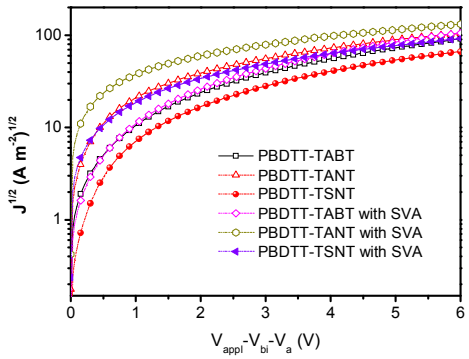

Fig. 8 $J^{1/2}$-V plots of copolymer:$PC_{71}BM$ (1:4) devices with or without the SVA treatments.

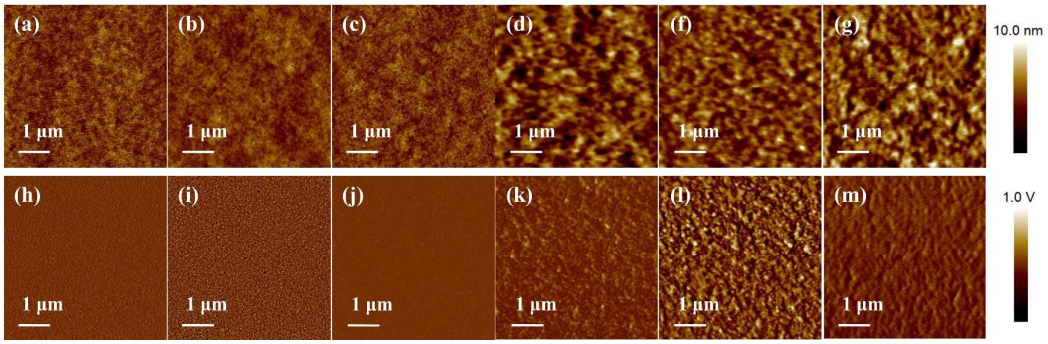

Fig. 9 AFM images of $PC_{71}BM$ blended with PBDTT-TABT, PBDTT-TANT and PBDTT-TSNT without the SVA (a, b, c) treatments and with the SVA (d, e, f) treatments, respectively.

Table 1 Polymerization results and thermal properties of copolymers.

Copolymer	Yield (%)	M_w (kDa)[a]	M_n (kDa)[a]	PDI[a]	T_d (°C)[b]
PBDTT-TABT	72.2	53.6	27.0	1.98	416
PBDTT-TANT	68.7	26.3	15.9	1.65	416
PBDTT-TSNT	61.9	24.5	13.5	1.80	360

[a]Molecular weights and polydispersity indices were determined by GPC in chloroform using polystyrene as standards. [b]Onset decomposition temperature measured by TGA under N2.

Table 2 Optical properties and electrochemical data of the copolymers.

Copolymer	Abs. (nm) λ_{max}^{sol}	Abs. (nm) λ_{max}^{film}	ε_{max}^{sol} (10^4) (M^{-1} cm^{-1})	E_g^{OPTa} (eV)	HOMO (eV)	LUMO (eV)	E_g^{CVb} (eV)
PBDTT-TABT	360, 490	376, 510	4.86	1.98	-5.45	-3.31	2.14
PBDTT-TANT	344, 492	355, 516	6.52	1.87	-5.37	-3.39	1.98
PBDTT-TSNT	348, 495	362, 518	5.18	1.85	-5.41	-3.44	1.97

Table 3 Photovoltaic parameters of the PSCs under AM 1.5G illumination (100 mW cm^{-2}).

Copolymer	Condition	V_{oc} (V)	J_{sc} (mA cm^{-2})	FF (%)	PCE_{max}/PCE_{ave} (%)	R_s (Ω cm^2)	R_{sh} (Ω cm^2)
PBDTT-TABT	as cast	1.00	9.64	47.5	4.60/4.52	15.6	322.4
	SVA	0.98	11.12	62.1	6.74/6.61	12.8	494.2
PBDTT-TANT	as cast	0.98	10.00	58.0	5.65/5.30	16.0	549.6
	SVA	0.95	13.06	65.2	8.04/7.84	10.8	629.2
PBDTT-TSNT	as cast	0.99	8.93	45.3	4.01/3.95	21.7	411.3
	SVA	0.96	10.25	60.9	6.00/5.96	14.7	601.8

Table 4 Hole mobility of copolymer:$PC_{71}BM$ blends with or without the SVA treatments.

Copolymer	Hole mobility($cm^2\ V^{-1}\ s^{-1}$)[a]	
	as cast	SVA
PBDTT-TABT	2.40×10^{-4}	3.28×10^{-4}
PBDTT-TANT	2.93×10^{-4}	3.94×10^{-4}
PBDTT-TSNT	1.33×10^{-4}	2.18×10^{-4}

[a]Hole only device structure: ITO/PEDOT:PSS/ polymer:$PC_{71}BM/MoO_3$/Au.

The table of contents entry

Synthesis and Photovoltaic Properties of Two-dimensional Benzodithiophene-thiophene Copolymers Pendant with Rational Naphtho[1,2-c:5,6-c]bis[1,2,5]thiadiazole Side Chains

Xiaopeng Xu, Kui Feng, Kai Li, Qiang Peng*

Key Laboratory of Green Chemistry and Technology of Ministry of Education, College of Chemistry, and State Key Laboratory of Polymer Materials Engineering, Sichuan University, Chengdu 610065, P. R. China

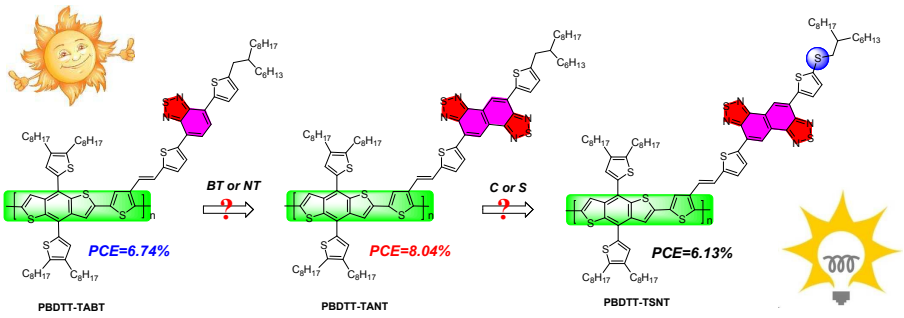

Rational molecular design of the conjugated side chains and solvent vapour annealing method were employed in this work to develop high performance two-dimensional copolymer donors and their efficient polymer solar cells .